SAND2016-11066C

Robust Bayesian Calibration of a RANS Model for Jet-in-Crossflow Simulations

Jaideep Ray * and Sophia Lefantzi †

Sandia National Laboratories, Livermore, CA 94550-0969,USA

Srinivasan Arunajatesan ‡ and Lawrence Dechant‡

Sandia National Laboratories, Albuquerque, NM 87185-5800, USA

Compressible jet-in-crossflow interactions are poorly simulated using Reynolds-Averaged Navier Stokes (RANS) equations. This is due to model-form errors (physical approximations) in RANS as well as the use of parameter values simply picked from literature (henceforth, the nominal values of the parameters). Previous work on the Bayesian calibration of RANS models has yielded joint probability densities of $\mathbf{C} = (C_\mu, C_{\epsilon 2}, C_{\epsilon 1})$, the most influential parameters of the RANS equations. The calibrated values were far more predictive than the nominal parameter values and the advantage held across a range of freestream Mach numbers and jet strengths. In this work we perform Bayesian calibration across a range of Mach numbers and jet strengths and compare the joint densities, with a view of determining whether compressible jet-in-crossflow could be simulated with a single joint probability density for C. We also compare the calibrated results to a recently developed analytical model of a jet-in-crossflow interaction. We find that probability densities for $C_{\epsilon 2}$ agree and also indicate that the range typically used in aerodynamic simulations should be extended. The densities for $C_{\epsilon 1}$ agree, approximately, with the nominal value. The densities for C_μ do not show any clear trend, indicating that they are not strongly constrained by the calibration observables, and in turn, do not affect them much. In the final paper, we will compare the predictive skill of the calibrated parameters against the analytical model as well as the density for C obtained in previous work. This will answer the question whether compressible jet-in-crossflow simulations can achieve acceptable accuracy using a different set of parameters (e.g., the one obtained from the analytical model) or whether a unique joint probability density for C could be applicable over a range of Mach number and jet strengths.

Nomenclature

$(\mathbf{u}_e, \mathbf{v}_e)$	Experimental counterpart of $(\mathbf{u}_m, \mathbf{v}_m)$
$(\mathbf{u}_m, \mathbf{v}_m)$	Modeled streamwise velocity deficit and normalized vertical velocities at probes
$(C_\mu, C_{\epsilon 2}, C_{\epsilon 1})$	Parameters in the $k - \epsilon$ RANS model requiring calibration
$\mathbf{C}_a$	Analytical estimates of $(C_\mu, C_{\epsilon 2}, C_{\epsilon 1})$
$\mathbf{C}_{nom}$	Nominal value of $(C_\mu, C_{\epsilon 2}, C_{\epsilon 1})$
$\mathcal{R}$	Physically realistic part of the parameter space
CVP	Counter-rotating vortex pair
JIC	Jet-in-crossflow

I. Introduction

Jet-in-crossflow interactions occur in a myriad of natural and engineering settings.[1] In aerodynamics, spin jets are often used to maneuver launch vehicles, setting up a compressible jet-in-crossflow interaction.

*Technical Staff, Quantitative Modeling and Analysis, MS 9159

†Technical Staff, Quantitative Modeling and Analysis, MS 9152, Senior Member

‡Technical Staff, Aerosciences Department, MS 0825, Senior Member

Experimental investigations[2] have shown that the exhaust from the spin rockets (the "jet") rolls into a complex configuration of counter-rotating vortex pairs (CVPs) that significantly modify the pressure distribution over the stabilizing fins of the flight vehicle. Detailed experimental investigations of compressible JIC interactions, for a range of Mach numbers and jet strengths, have been performed experimentally,[3,4,5] referred to here as the "Beresh" experiments. They have been compared to simulations performed using Reynolds-Averaged Navier Stokes (RANS) models.[6] These comparisons show that RANS simulations have poor predictive skill - the simulated jet rolls into a CVP that is far too strong and penetrates into the freestream far more than what is observed in experimental data. These predictive errors arise from two sources. The first concerns model-form errors i.e., due to approximations of turbulence physics in RANS equations. The second source of errors is the use of parameters in RANS equations simply picked from literature, which are often derived by calibrating to canonical incompressible flows. It is unclear which is the larger source of predictive uncertainty.

One way of improving the predictive skill of RANS in JIC simulations is to obtain calibrated parameters. Due to the model-form errors and limited experimental data, it is not always possible to estimate these parameters with much certainty. Consequently, Bayesian calibration techniques are used, as they model the parameters to be estimated as random variables and infer their probability density functions (PDFs) from observational data. The PDFs capture the uncertainty in the estimation. Bayesian estimation of $k-\epsilon$ RANS models has been performed for flow over flat plates under favorable and adverse pressure gradients[7] and for turbulent flow in urban canyons.[8] Alternatively, one may assume that the poor predictive skill of RANS equations may be ameliorated by augmenting some of the model equations with a spatially variable source term which is learned by calibrating (i.e., full-field inversions for the source term) to high-fidelity data e.g., Direct Numerical Simulation solutions of flows similar to the flow of interest. The dependence of the source term on local flow properties is then learned using the calibrated RANS solutions as the training data. This approach has been used for 2D flows over bumps in channels and airfoils.[9,10,11,12]

A completely different way of improving the predictive skill of RANS JIC simulations is to develop expressions/estimates of critical parameters via an *analytical* approach. In a companion paper,[13] we derive a self-similar solution of the jet (after a JIC interaction) that is applicable in the farfield and obtain estimates of 3 $k-\epsilon$ parameters $\mathbf{C} = (C_\mu, C_{\epsilon 2}, C_{\epsilon 1})$ analytically, without using Beresh measurements and without performing any type of fitting. Thus these measurements are free of any conflating of model-form and parametric inadequacies. The parameter estimates $\mathbf{C}_a = \{0.1, 2.0, 1.34\}$ are somewhat different from the nominal values of the parameters $\mathbf{C}_{nom} = \{0.09, 1.92, 1.44\}$ typically used in $k-\epsilon$ RANS simulations, but produced predictions of the flowfield that were significantly better than those obtained using $\mathbf{C}_{nom}$. This determination was performed using the Beresh experimental data.

In a previous paper[14] we addressed the Bayesian calibration of compressible JIC interactions using data from one of the Beresh experiments. The experiment consists of introducing a Mach number $M = 3.73$ jet of 9.53 mm diameter into a $M = 0.8$ freestream in a wind tunnel test section. The jet-to-freestream momentum ratio J is 10.2. The jet bends into the flow and rolls into a CVP as it flows downstream. PIV (velocity) measurements are available on the mid-plane, the longitudinal plane of symmetry and a transverse/cross plane that slices through the CVP. Experimentally measured vorticity on the crossplane was used, via Bayesian calibration, to obtain a 3D joint PDF (JPDF) for $\mathbf{C} = (C_\mu, C_{\epsilon 2}, C_{\epsilon 1})$, the parameters to which the flow was found to be most sensitive. An optimal parameter set $\mathbf{C}_{opt} = \{0.1025, 2.099, 1.416\}$ was also obtained, which is quite different from $\mathbf{C}_{nom}$. Samples of $\mathbf{C}$ drawn from the calibrated JPDF provided predictions of the flowfield that were far more accurate than those obtained using $\mathbf{C}_{nom}$; this was verified by comparing with (Beresh) experimental velocity measurements on the midplane and crossplane. The improvement in predictive skill was retained, when examined against experimental data, at other M and J values, though the agreement was not as good as the $M = 0.8, J = 10.2$ case.

Clearly, then, $\mathbf{C}_a$, $\mathbf{C}_{opt}$ and the calibrated JPDF from the $(M = 0.8, J = 10.2)$ calibration study are all more predictive than $\mathbf{C}_{nom}$. However the predictive skill of $\mathbf{C}_{opt}$ and the calibrated JPDF from the $(M = 0.8, J = 10.2)$ calibration study is seen to drop as we apply them to (M, J) combinations other than $(0.8, 10.2)$. It is unknown whether this drop in predictive skill is significant compared to that of a $\mathbf{C}$ obtained via calibration to experimental data. In this study we perform calibration for $\mathbf{C}$ for five (M, J) combinations and compare its predictive skill versus $\mathbf{C}_a$ and $\mathbf{C}_{opt}$ obtained from the $(M = 0.8, J = 10.2)$ calibration study. The ultimate aim of this study is to find a replacement for $\mathbf{C}_{nom}$ in $k-\epsilon$ simulations of compressible JIC interactions that is robust across a $M-J$ range.

II. Problem formulation

II.A. Experimental and computational setup

The experimental and computational setup used in this calibration study have been described fully elsewhere[14] and we provide a summary below. The data used here is obtained from a set of wind tunnel experiments conducted by Beresh et al.[3,4] . A schematic of the test section is shown in Fig. 1. The experiments involve injecting a M = 3.73 jet, of diameter 9.53 mm, into a freestream from the bottom of the test section. The freestream Mach number is denoted M and the ratio of jet-to-freestream momenta is J. Experiments are conducted for $M = 0.6, 0.7$ and 0.8 while $J = 10.2$. For $M = 0.8$, experiments are conducted at $J = 16.7$ and 5.6, in addition to 10.2. The jet bends into the freestream and rolls into a CVP. PIV measurements are made on two planes, as shown in Fig. 1. The plane of symmetry is called the midplane, whereas the transverse plane slicing through the CVP is called the crossplane. Velocity measurements are available on the midplane for all the five experimental datasets being considered in this study. Velocity measurements (and therefore streamwise vorticity) are available only for the three $M = 0.8$ test cases (i.e., for $J = 5.6, 10.2, 16.7$) and was used as the calibration observable in our previous work.[14] Since we will perform calibration for all five (M, J) combinations, we will use measurements of streamwise velocity u and vertical velocity v on the midplane as our calibration observable. Measurements on the midplane are made at 5 stations, with the first station being 200 mm downstream of the jet and the rest at intervals of 50 mm. At each location, measurements are made at 63 vertically distributed points called "probes". The crossplane is 321.8 mm downstream of the jet.

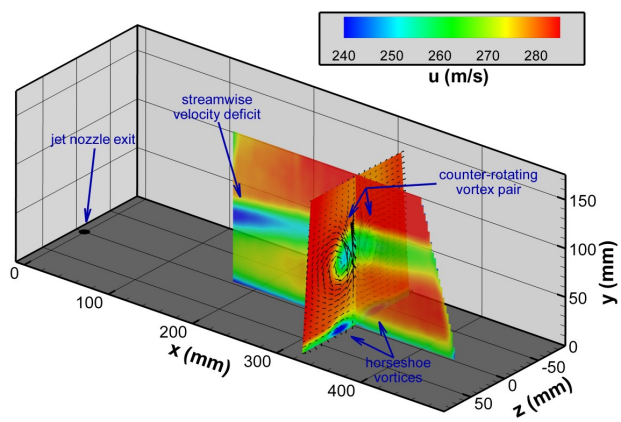

Figure 1. Schematic of the test section showing the orifice where the jet is introduced and the mid- and crossplane where experimental measurements are made.

The calibration is performed using the compressible form of the $k - \epsilon$ RANS equation[15] and is fully described in Ref. 14. The most important parameters that affect the flowfield are $(C_\mu, C_{\epsilon 2}, C_{\epsilon 1})$, which we will refer to as $\mathbf{C}$. Our flow solver, SIGMA CFD (Sandia Implicit Generalized Mult-Block Analysis Code for Fluid Dynamics), uses a Roe-TVD flux scheme with a minmod limiter for spatial discretization. Time integration is carried out using a first order point-implicit scheme. The calculations are initialized using a first-order spatial scheme, time-marched for 5000 timesteps, and relaxed to convergence using the second order scheme for 25000 timesteps. Time marching to steady state was carried out using local time stepping with a gradual CFL ramp to accelerate convergence. A multi-block mesh with approximately 10 million grid cells is used; mesh convergence studies are in Ref. 6. Details of initial and boundary conditions and mesh refinement near the walls are in Ref. 14.

II.B. The inverse problem

Let $\mathbf{y}_e$ be a vector (of length N_p) of experimental observations, measured at a set of N_p locations ("probes"). Let $\mathbf{y}_m(\mathbf{C})$ be model predictions of the same, produced by a parameter setting $\mathbf{C}$. They are related by $\mathbf{y}_e = \mathbf{y}_m(\mathbf{C}) + \boldsymbol{\epsilon}$ where $\boldsymbol{\epsilon}$ is a combination of measurement and model-form error. We make a modeling assumption that the errors at the probes are uncorrelated, independently and identically distributed as a

zero-mean Gaussian i.e. $\boldsymbol{\epsilon} = \{\epsilon_i\}, \epsilon_i \sim \mathcal{N}(0, \sigma^2)$. σ^2 thus provides a crude measure of the model - data misfit after calibration. If the measurement errors are low, σ^2 provides an estimate of the model-form error.

Let $P(\mathbf{C}, \sigma^2|\mathbf{y}_e)$ be the joint probability density function of the parameters and the model - data misfit, conditional on the observed data $\mathbf{y}_e$. Let $\Pi_1(\mathbf{C})$ and $\Pi_2(\sigma^2)$ be our prior belief regarding the distribution of $\mathbf{C}$ and σ^2. The likelihood of observing $\mathbf{y}_e$, given a parameter setting $\mathbf{C}$, $\mathcal{L}(\mathbf{y}_e|\mathbf{C})$, is given by

$$\mathcal{L}(\mathbf{y}_e|\mathbf{C}, \sigma^2) \propto \frac{1}{\sigma^{N_p}} \exp\left(-\frac{||\mathbf{y}_e - \mathbf{y}_m(\mathbf{C})||_2^2}{2\sigma^2}\right).$$

By Bayes' theorem, the calibrated distribution (or posterior distribution) of $(\mathbf{C}, \sigma^2)$ can be given as

$$P(\mathbf{C}, \sigma^2|\mathbf{y}_e) \propto \mathcal{L}(\mathbf{y}_e|\mathbf{C}, \sigma^2)\ \Pi_1(\mathbf{C})\ \Pi_2(\sigma^2) \propto \frac{1}{\sigma^{N_p}} \exp\left(-\frac{||\mathbf{y}_e - \mathbf{y}_m(\mathbf{C})||_2^2}{2\sigma^2}\right)\ \Pi_1(\mathbf{C})\ \Pi_2(\sigma^2) \tag{1}$$

The actual model outputs i.e., components of $\mathbf{y}_m$, are the streamwise velocity deficit u_{def} and normalized velocity v_{norm} defined as

$$u_{def} = 1 - \frac{u}{U_{max}(x)} \qquad v_{norm} = \frac{v}{U_\infty},$$

where U_{max} is the maximum streamwise velocity at an x-location and U_∞ is the freestream velocity. Let $\mathbf{u}_m$ be the predicted *streamwise velocity deficit* u_{def} and $\mathbf{v}_m$ be the *normalized vertical velocity* v_{norm} for all the probes . Let $\mathbf{u}_e$ and $\mathbf{v}_e$ be their experimental counterparts over all the probes . The specific form of Eq. 1 used in this study is:

$$P(\mathbf{C}, \sigma^2|\mathbf{u}_e, \mathbf{v}_e) \propto \frac{1}{\sigma^{N_p}} \exp\left(-\frac{||(\mathbf{u}_e - \mathbf{u}_m(\mathbf{C}))/K_u||_2^2}{2\sigma^2}\right)\ \exp\left(-\frac{||(\mathbf{v}_e - \mathbf{v}_m(\mathbf{C}))/K_v||_2^2}{2\sigma^2}\right)\ \Pi_1(\mathbf{C})\ \Pi_2(\sigma^2), \tag{2}$$

where $K_u = \max(\mathbf{u}_e)$ and $K_v = \max(\mathbf{v}_e)$. Normalization of the model-data mismatch using K_u, K_v ensures that the contributions from u_{def} and v_{norm} are equally weighted in the expression for the posterior distribution.

As in Ref. 14, the inverse problem is solved via sampling. We use a Markov chain Monte Carlo (MCMC) method called Delayed Rejection Adaptive Metropolis (DRAM; Ref. 16), as implemented in the R[17] package `FME`[18] to draw samples of $\{\mathbf{C}, \sigma^2\}$. We reconstruct $P(\mathbf{C}, \sigma^2|\mathbf{y}_e)$ empirically by kernel density estimation.[19] The prior density for σ^2 is defined in terms of its reciprocal i.e., $\Pi_2(\sigma^{-2})$ and is modeled using a Gamma prior i.e., $\sigma^{-2} \sim \Gamma(k, \theta)$, where $k = 1, \theta = 1$. The inverse Gamma prior for σ^2 is a conjugate prior which simplifies sampling of σ^{-2} via a Gibbs sampler. Also, the prior is virtually non-informative for $\sigma^2 > 5$. Raftery-Lewis method[20] implemented in the R package `mcgibbsit`.[21] The MCMC method requires $O(10^4)$ samples to construct $P(\mathbf{C}, \sigma^2|\mathbf{y}_e)$, each of which requires a 3D RANS model evaluation to provide $\mathbf{y}_m(\mathbf{C})$. Since this is impractical, we will develop a surrogate model, a polynomial that maps the dependence of our calibration variables $(\mathbf{u}_m, \mathbf{v}_m)$ on $\mathbf{C}$. The surrogate model will serve as a computationally inexpensive proxy for SIGMA CFD. We consider the following bounds on $\mathbf{C}$ taken from Ref. 15:

$$0.06 \le C_\mu \le 0.12, \qquad 1.7 \le C_{\epsilon 2} \le 2.1, \qquad \text{and} \qquad 1.2 \le C_{\epsilon 1} \le 1.7. \tag{3}$$

II.C. Priors and surrogates

An informative prior: While it is tempting to combine the bounds in Eq. 3 into a uniform distribution in the cuboid $\mathcal{C}$ in $(C_\mu, C_{\epsilon 2}, C_{\epsilon 1})$ space, we shall refrain from doing. Arbitrary combinations of $(C_\mu, C_{\epsilon 2}, C_{\epsilon 1})$ from $\mathcal{C}$ may not be physical, and consequently, we will use the discrepancy $\mathbf{y}_e - \mathbf{y}_m(\mathbf{C})$ to choose a physically realistic region $\mathcal{R} \subset \mathcal{C}$ to serve as $\Pi_1(\mathbf{C})$. Details on how $\Pi_1(\mathbf{C})$ is constructed are in Ref. 14 and we provide a summary here.

Constructing the surrogates requires us to generate a training dataset that captures the variation of $\mathbf{u}_m$ and $\mathbf{v}_m$ over $\mathcal{C}$. We draw 2744 $(= 14^3)$ samples of $\mathbf{C}$ from $\mathcal{C}$ using a quasi Monte Carlo space-filling (Halton sequence) method and conduct 3D RANS simulations with them using SIGMA CFD. Many of the samples are non-physical and the simulations do not converge to a steady state. Others (2628 samples) do, but yield flowfields that are quite unlike transonic, high Reynolds number flows. In order to isolate values of $\mathbf{C}$ that yield realistic flowfields we compute the RMS (root mean square) error between $(\mathbf{u}_e, \mathbf{v}_e)$ and $(\mathbf{u}_m, \mathbf{v}_m)$for all the successful simulations and preserve the top 25%, resulting in $0.25 \times 2628 = 657$ samples. A random subset

of these $\mathbf{C}$ samples are plotted in Fig. 2 (left) and occupy a certain section of $\mathcal{C}$ i.e., they are not uniformly scattered in $\mathcal{C}$. This is the physically realistic part of $\mathcal{C}$, called $\mathcal{R}$, and forms the basis of constructing the prior density $\Pi_1(\mathbf{C})$. As in Ref. 14, we define

$$\Pi_1(\mathbf{C}) = \begin{cases} 1 & \text{if } \mathbf{C} \in \mathcal{R} \\ 0 & \text{otherwise} \end{cases} \tag{4}$$

The 2628 successful runs (of which 657 mark out $\mathcal{R}$) are used to train a binary support vector machine classifier. The procedure and software to do so are in Ref. 14. A misclassification rate less than 10% is a requirement for building a successful classifier. The classifier is used as the implementation of the prior $\Pi_1(\mathbf{C})$ as described in Eq. 4 and is used within the MCMC procedure to infer the posterior density $P(\mathbf{C}, \sigma^2|\mathbf{u}_e, \mathbf{v}_e)$.

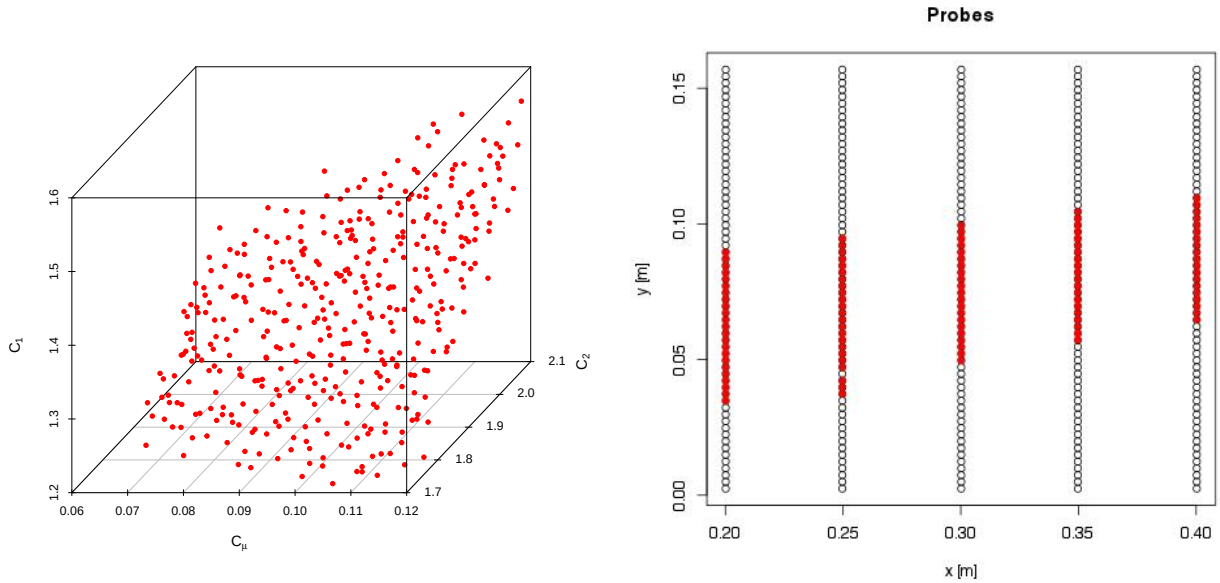

Figure 2. Left: A set of C points in $\mathcal{C}$ that produce physically realistic flowfields i.e., they approximately mark out $\mathcal{R}$. Right: A plot of the probes on the midplane where experimental data are available. The filled circles are the probes for which we could build accurate surrogate models. They track the spatial evolution of the CVP, and do not cover the boundary layer at the test section walls..

Surrogate models: A surrogate model is defined as a polynomial curve-fit between a model prediction at a probe i.e., u_{def} and v_{norm}, that captures their dependence on $\mathbf{C}$. We use the samples of $\mathbf{C}$ that define $\mathcal{R}$, and the flowfields they yield, to learn the polynomial model. The procedure is described in detail Ref. 14. We start with a cubic polynomial in $(C_\mu, C_{\epsilon 2}, C_{\epsilon 1})$ space to map $\mathbf{C}$ to u_{def} (or v_{norm}). The fitting is performed via least-squares regression and simplified via incrementally dropping terms and computing the Akaike Information Criterion. Many cubic terms are removed and, for a few probes, the surrogate reduces to a quadratic one. However, simply being able to construct a surrogate does not imply that it is accurate. As in Ref. 14, we compute the predictive error of the surrogate via repeated random sub-sampling validation (a form of cross validation) and retain only those probes whose surrogate models have less than 15% error (for both u_{def} and v_{norm}). In Fig. 2 (right) we plot the probes on the midplane that were retained for the $(M = 0.8, J = 10.2)$ case. As the figure shows, of the $63 \times 5 = 315$ probes for which we have experimental measurements, we could make surrogate models (of acceptable accuracy) for only 107. These "model-able" probes follow the trajectory of the CVP. Note that we do not keep any probes in the boundary layer - the calibration is simply aimed at simulating the jet and its roll-up accurately.

Obtaining correct JPDFs: Having implemented the prior $\Pi_1(\mathbf{C})$ via a classifier and constructed polynomial surrogates for $\mathbf{u}_m$ and $\mathbf{v}_m$, we solve the inverse problem (Eq. 2) for the posterior density $P(\mathbf{C}, \sigma^2|\mathbf{u}_e, \mathbf{v}_e)$. We plot the marginalized posterior and prior PDFs in Fig. 3. For comparison, we also plot the marginalized PDFs obtained using measurements of vorticity on the crossplane[14] for the same interaction. We see that the two posterior PDFs are close but not identical. Further, the priors that we use here (plotted using $\circ$) are different from those used in our previous study,[14] plotted with $\triangle$. This is especially

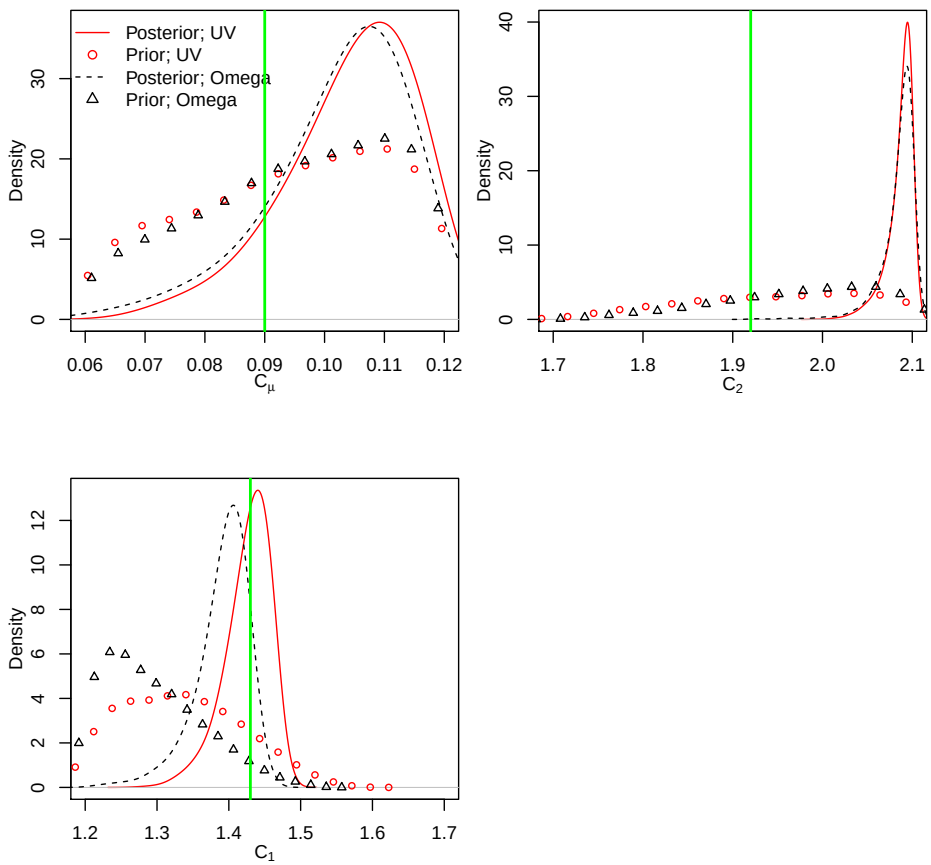

Figure 3. Marginalized posterior PDFs of C_μ, $C_{\epsilon 2}$ and $C_{\epsilon 1}$ as inferred using $(\mathbf{u}_e, \mathbf{v}_e)$ (marked "UV") and using streamwise vorticity (marked "Omega"). The corresponding priors are plotted using symbols. The vertical line is the nominal value.

true for $C_{\epsilon 1}$. The comparison ensures that (1) $(\mathbf{u}_e, \mathbf{v}_e)$ are as informative about $(C_\mu, C_{\epsilon 2}, C_{\epsilon 1})$ as vorticity on the crossplane and (2) the classifier and surrogates were constructed with a degree of accuracy that is comparable to our previous work.[14] Therefore, the calibration methodology using $(\mathbf{u}_e, \mathbf{v}_e)$, as described above, can be applied to other JIC interactions i.e., those with different (M, J) combinations.

III. Results

In Fig. 4 we plot the marginalized PDFs (i.e., $P(\mathbf{C}, \sigma^2 | \mathbf{u}_e, \mathbf{v}_e)$) obtained for JIC interactions corresponding to $(M, J) = (0.6, 10.2), (0.7, 10.2), (0.8, 10.2), (0.8, 16.7)$ and $(0.8, 5.6)$. The nominal values $\mathbf{C}_{nom}$ are plotted using dashed vertical lines and the analytical estimate $\mathbf{C}_a$ using a solid vertical line. It is clear that $C_{\epsilon 2}$ is much higher that the nominal value and one could argue that the upper bound for $C_{\epsilon 2}$ should be increased to allow a better calibration. The nominal estimate for $C_{\epsilon 1}$ agrees with the peak for many of the calibration cases except for the $(0.6, 10.2)$ case. The PDFs for C_μ do not show any consistent trend, though one we do see 3 peaks in the region $C_\mu > 0.11$. The analytical estimate for $C_{\epsilon 2}$ and C_μ are closer to the calibrated values than the nominal one; whereas the opposite holds true for $C_{\epsilon 1}$. The three parameters exert different degrees of influence on the flowfield and it is unclear whether the predictive skill of $\mathbf{C}_a$ may be similar to the calibrated JPDF. We have already shown that $\mathbf{C}_a$ is more predictive than $\mathbf{C}_{nom}$.[13] Post-calibration, the residual model-data mismatch (quantified by σ) is also plotted in Fig. 4; it is clear that the $(M = 0.6, J = 10.2)$ has the worst fit whereas the $(M = 0.8, J = 10.2)$ and $(M = 0.7, J = 10.2)$ have the best fits (lower σ).

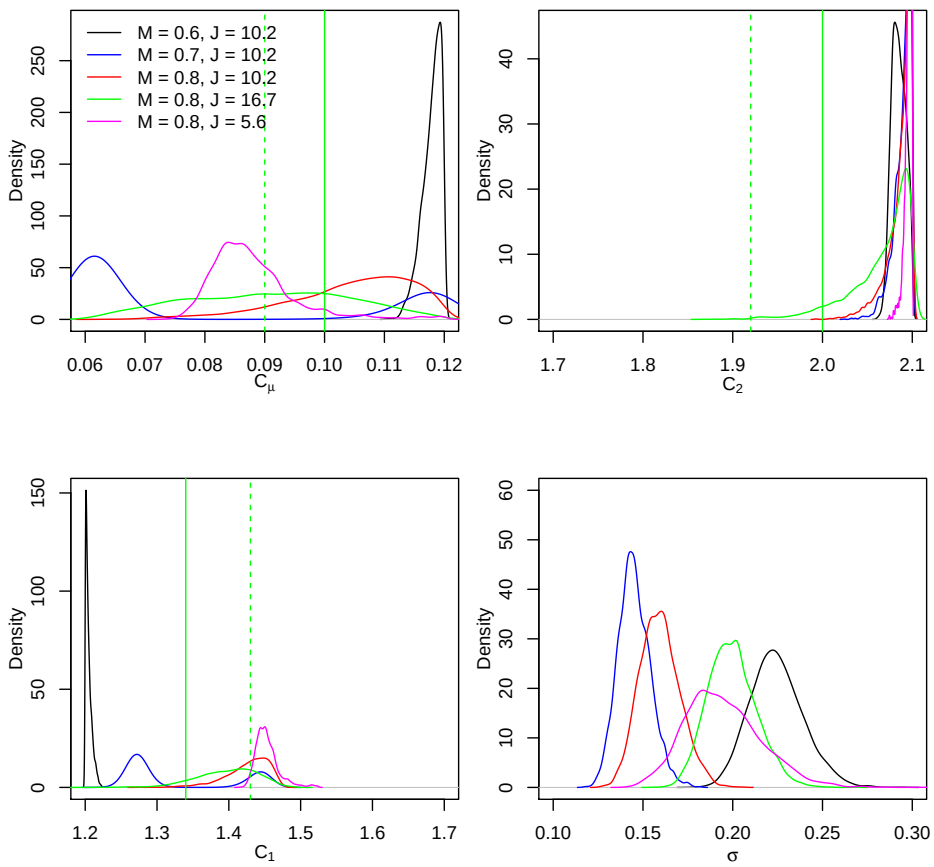

Figure 4. Marginalized posterior PDFs inferred for JIC interactions corresponding to five different (M, J) combinations. The dashed vertical line is $\mathbf{C}_{nom}$ whereas the solid line is the analytical estimate $\mathbf{C}_a$.

IV. Conclusions

In the final paper, we will investigate the following questions:

1. We will investigate if the predictive skill of $(C_\mu, C_{\epsilon 2}, C_{\epsilon 1})$, as inferred from $(\mathbf{u}_e, \mathbf{v}_e)$, is comparable to that inferred in our previous paper.[14] We will do so by performing a posterior predictive test and plotting the velocities/vorticities on the midplane/crossplane, along with the experimental data.

2. We will quantify the degree of variation achieved in the flowfield due to the uncertainty in $(C_\mu, C_{\epsilon 2}, C_{\epsilon 1})$. This will also quantify the importance of σ in bracketing the experimental data when conducting simulations using parameters sampled from the posterior JPDF.

3. We will compare the predictive skills of the JPDF, $\mathbf{C}_a$ and $\mathbf{C}_{nom}$ versus experimental data. This is to mostly to check whether $\mathbf{C}_a$ can be used as a convenient approximation to the calibrated JPDF in future RANS simulation.

Acknowledgment

This work was supported by Sandia National Laboratories' Advanced Scientific Computing (ASC) Verification and Validation program. Sandia National Laboratories is a multi-program laboratory managed and operated by Sandia Corporation, a wholly owned subsidiary of Lockheed Martin Corporation, for the U. S. Department of Energy's National Nuclear Security Administration under contract DE-AC04-94AL85000.

References

[1]Mahesh, K., "The interaction of jets with crossflows," *Annual Reviews of Fluid Mechanics*, Vol. 45, 2013, pp. 379–407.

[2]Beresh, S. J., Heineck, J. T., Walker, S. M., Schairer, E. T., and Yaste, D. M., "Planar velocimetry of jet/fin interaction on a full-scale flight vehicle configuration," *AIAA Journal*, Vol. 45, No. 8, 2007, pp. 1827–1840.

[3]Beresh, S. J., Henfling, J. F., Erven, R. J., and Spillers, R. W., "Penetration of a transverse supersonic jet into a subsonic compressible crossflow," *AIAA Journal*, Vol. 43, No. 2, 2005, pp. 379–389.

[4]Beresh, S. J., Henfling, J. F., Erven, R. J., and Spillers, R. W., "Crossplane velocimetry of a transverse supersonic jet in a transonic crossflow," *AIAA Journal*, Vol. 44, No. 12, 2006, pp. 3051–3061.

[5]Beresh, S. J., Henfling, J. F., Erven, R. J., and Spillers, R. W., "Turbulent characteristics of a transverse supersonic jet in a subsonic compressible crossflow," *AIAA Journal*, Vol. 43, No. 11, 2005, pp. 2385–2394.

[6]Arunajatesan, S., "Evaluation of two-equation RANS models for simulation of jet-in-crossflow problems," *50th AIAA Aerospace Sciences Meeting*, 2012.

[7]Edeling, W. N., Cinnella, P., Dwight, R. P., and Bijl, H., "Bayesian estimates of parameter variability in $k-\epsilon$ turbulence model," *Journal of Computational Physics*, Vol. 258, 2014, pp. 73–94.

[8]Guillas, S., Glover, N., and Malki-Epshtein, L., "Bayesian calibration of the constants of the $k-\epsilon$ turbulence model for a CFD model of street canyon flow," *Computer Methods in Applied Mechanics and Engineering*, Vol. 279, 2014, pp. 536–553.

[9]Duraisamy, K., Zhang, Z. J., and Singh, A. P., "New approaches in turbulence and transition modeling using data-driven techniques," *Proceedings of the 53rd AIAA Aerospace Sciences Meeting, Kissimmee, FL*, 2015, Paper No. AIAA-2015-1284.

[10]Tracey, B., Duraisamy, K., and Alonso, J. J., "A machine learning strategy to assist turbulence model development," *Proceedings of the 53rd AIAA Aerospace Sciences Meeting, Kissimmee, FL*, 2015, Paper No. AIAA-2015-1287.

[11]Zhang, Z. J. and Duraisamy, K., "Machine learning methods for data-driven turbulence modeling," *Proceedings of the 22nd AIAA Computational Fluid Dynamics Conference*, 2015, Paper No. AIAA-2015-2460.

[12]Parish, E. and Duraisamy, K., "Quantification of turbulence modeling uncertainties using full field inversions," *Proceedings of the 22nd AIAA Computational Fluid Dynamics Conference*, 2015, Paper No. AIAA-2015-2459.

[13]DeChant, L., Ray, J., Lefantzi, S., Ling, J., and Arunajatesan, S., "$k-\epsilon$ Turbulence Model Parameter Estimates Using an Approximate Self-similar Jet-in-Crossflow Solution," 2016, Submitted, AIAA Aviation 2017.

[14]Ray, J., Lefantzi, S., Arunajatesan, S., and Dechant, L., "Bayesian Parameter Estimation of a $k-\epsilon$ Model for Accurate Jet-in-Crossflow Simulations," *AIAA Journal*, Vol. 54, No. 8, 2016, pp. 2432–2448.

[15]Brinckman, K. W., Calhoon, W. H., and Dash, S. M., "Scalar fluctuation modeling for high-speed aeropropulsive flows," *AIAA Journal*, Vol. 45, No. 5, 2007, pp. 1036–1046.

[16]Haario, H., Laine, M., Mira, A., and Saksman, E., "DRAM-Efficient adaptive MCMC," *Statistics and Computing*, Vol. 16, No. 4, 2006, pp. 339–354.

[17]R Core Team, *R: A Language and Environment for Statistical Computing*, R Foundation for Statistical Computing, Vienna, Austria, 2012, ISBN 3-900051-07-0.

[18]Soetaert, K. and Petzoldt, T., "Inverse Modelling, Sensitivity and Monte Carlo Analysis in R Using Package FME," *Journal of Statistical Software*, Vol. 33, No. 3, 2010, pp. 1–28.

[19]Silverman, B. W., *Density Estimation for Statistics and Data Analysis*, Chapman and Hall, 1986.

[20]Raftery, A. and Lewis, S. M., "Implementing MCMC," *Markov Chain Monte Carlo in Practice*, edited by W. R. Gilks, S. Richardson, and D. J. Spiegelhalter, Chapman and Hall, 1996, pp. 115–130.

[21]Warnes, G. R. and with contributions by Robert Burrows, *mcgibbsit: Warnes and Raftery's MCGibbsit MCMC diagnostic*, 2011, R package version 1.0.8.